AMERICAN SOCIETY FOR MICROBIOLOGY | Applied and Environmental Microbiology®

ENVIRONMENTAL MICROBIOLOGY

Structural and Functional Dynamics of Soil Microbes following Spruce Beetle Infestation

Gordon F. Custer,[a,b,c] Linda T. A. van Diepen,[b,c] William L. Stump[a]

[a]Department of Plant Sciences, University of Wyoming, Laramie, Wyoming, USA
[b]Department of Ecosystem Science and Management, University of Wyoming, Laramie, Wyoming, USA
[c]Program in Ecology, University of Wyoming, Laramie, Wyoming, USA

ABSTRACT As the range of bark beetles expands into new forests and woodlands, the need to understand their effects on multiple trophic levels becomes increasingly important. To date, much attention has been paid to the aboveground processes affected by bark beetle infestation, with a focus on photoautotrophs and ecosystem level processes. However, indirect effects of bark beetle on belowground processes, especially the structure and function of soil microbiota remains largely a black box. Our study examined the impacts of bark beetle-induced tree mortality on soil microbial community structure and function using high-throughput sequencing of the soil bacterial and fungal communities and measurements of extracellular enzyme activities. The results suggest bark beetle infestation affected edaphic conditions through increased soil water content, pH, electrical conductivity, and carbon/nitrogen ratio and altered bulk and rhizosphere soil microbial community structure and function. Finally, increased enzymatic activity suggests heightened microbial decomposition following bark beetle infestation. With this increase in enzymatic activity, nutrients trapped in organic substrates may become accessible to seedlings and potentially alter the trajectory of forest regeneration. Our results indicate the need for incorporation of microbial processes into ecosystem level models.

IMPORTANCE Belowground impacts of bark beetle infestation have not been explored as thoroughly as their aboveground counterparts. In order to accurately model impacts of bark beetle-induced tree mortality on carbon and nutrient cycling and forest regeneration, the intricacies of soil microbial communities must be examined. In this study, we investigated the structure and function of soil bacterial and fungal communities following bark beetle infestation. Our results show bark beetle infestation to impact soil conditions, as well as soil microbial community structure and function.

KEYWORDS bacteria, bark beetle, community dynamics, *Dendroctonus*, ectomycorrhizae, extracellular enzymes, fungi, microbial ecology, microbial function, *Picea engelmanii*

Increased mean winter temperatures and changes in precipitation patterns coupled with current management practices of western United States forests have provided an increasingly hospitable environment for epidemic-level bark beetle outbreaks (1–3). The current outbreak of spruce beetle (*Dendroctonus rufipennis*) in the intermountain region of the western United States began in the late 1980s and has affected upwards of 500,000 ha of Engelmann spruce (*Picea engelmanii*) in Wyoming and Colorado alone (4). Bark beetle, like other major landscape level disturbances such as fire or logging, has the potential to rapidly impact large areas of forests. However, while these disturbances are similar in scale, bark beetle infestation is unique in many ways. The most dramatic difference is the fact that with bark beetle all vegetation biomass

Citation Custer GF, van Diepen LTA, Stump WL. 2020. Structural and functional dynamics of soil microbes following spruce beetle infestation. Appl Environ Microbiol 86:e01984-19. https://doi.org/10.1128/AEM.01984-19.

Editor Claire Vieille, Michigan State University

Address correspondence to Gordon F. Custer, gcuster@uwyo.edu.

Received 28 August 2019
Accepted 10 November 2019
Accepted manuscript posted online 15 November 2019
Published 21 January 2020

remains in the system and provides a large one-time input of nitrogen-rich needles (5), followed by gradual input of woody debris and root decay, sometimes taking upwards of 50 years until snag fall (defined as when the trunk falls to the ground) (6). In addition, bark beetle infestation creates a forest with decreased canopy cover, increased soil moisture (7), decreased shallow fine root biomass (8), and changes in carbon (C) and nitrogen (N) inputs and cycling (5, 7–9), leading to altered edaphic conditions in forested ecosystems.

The altered edaphic conditions caused by bark beetle-induced tree mortality have the potential to impact soil microbial community structure and function (10–13). Since microbes are known to play an integral role in many ecosystem processes, including decomposition and nutrient cycling (7, 9), understanding the response of microbial communities to bark beetle infestation is important. Across the Northern Hemisphere, studies have examined microbial dynamics following bark beetle infestation revealing changes in microbial functioning (10) and community structure (10, 12–14), and specifically a decrease in symbiotic fungal taxa (10, 12). However, conflicting results exist, for example, Ferrenberg et al. (15) found no changes in soil bacterial community structure in the first 5 years following mountain pine beetle-induced tree mortality in the southern Rocky Mountains. A shortcoming of these microbial studies is that they address changes to community structure in soil and/or litter following bark beetle infestation, neglecting to consider microbial dynamics in the bulk and rhizosphere soil compartments individually, and more often than not, only one kingdom is studied, and community data are not paired with microbial functional measurements. While dynamic microbial communities following insect-induced tree mortality are expected (10–14), the high level of functional redundancy inherent in the soil microbiome poses the question of whether changes in community structure will result in changes in functionality. This question should be regarded with utmost importance due to the fact microbes represent a significant source of CO_2, releasing upward of 50 to 75 Pg per year into the atmosphere (16).

Though research has been conducted on microbiome responses to bark beetle infestation in soil, examining the response of soil microbes in the rhizosphere and bulk soil individually has been neglected. While close in proximity to bulk soil, the rhizosphere provides a unique, stable, and nutrient-rich (17, 18) environment within the soil matrix for microbes to thrive. Plants recruit soil microbes into the rhizosphere by exuding labile carbon in an attempt to culture a beneficial microbial community (17, 18), including mutualistic species such as mycorrhizal fungi. However, once unable to provide resources to the rhizosphere community, the formerly stable environment experiences turnover, opening the door for root pathogens, saprotrophs, and other potentially detrimental taxa to become established and reducing mutualistic mycorrhizal taxa. This shift in fungal rhizosphere community composition was observed under drought-induced tree mortality in a Mediterranean climate (19), and whether or not this trend is common to other climates and disturbances is yet to be determined. Thus, the response of rhizosphere microbiota to disturbance remains a black box and presents an opportunity for novel ecological research.

We expected that the microbial community, both fungi and bacteria, to be significantly different in the rhizosphere compared to the bulk soil due to the changes in rhizodeposits and decaying root mass across the entire chronosequence. Both the rhizosphere and bulk soil communities should experience rapid turnover following beetle kill, resulting in a decrease in mutualistic taxa and a relative increase in pathogenic and saprotrophic taxa, as was found in Hopkins et al. (19). Finally, with the hypothesized changes in microbial community structure, as measured by high-throughput sequencing, we expect an altered functional profile as measured by soil extracellular enzyme activities, with the highest potential for decomposition occurring following needle drop and root death in the clusters of infested and dead trees in our woodland system.

With this framework in mind, we set out to address the following questions about soil microorganisms and their responses to disturbance. (i) When expected shifts in

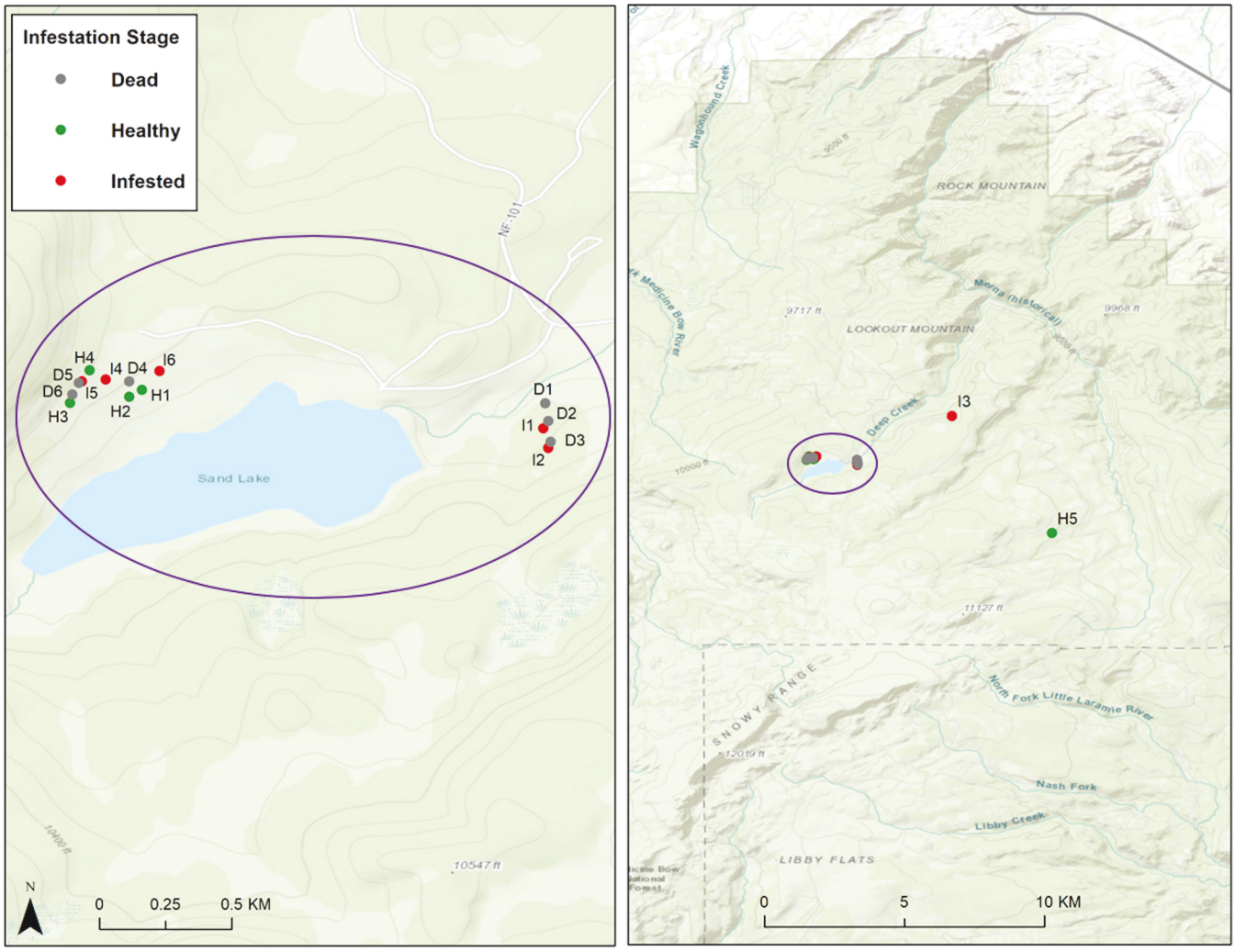

FIG 1 Locations of selected tree clusters. Clusters are indicated by dots colored by their infestation stage. Two instances exist in which the distance between two sites are <30 m (clusters I2:D3 and I5:D5). The left side of the figure provides a zoomed in view of the majority of the samples, while the right provides an overview. The purple ellipse surrounds the same sites in both images.

community structure occur following beetle infestation, what groups of taxa are driving these community differences and are similar patterns observed in the rhizosphere and bulk soil compartments? (ii) With expected altered edaphic conditions and microbial community structure following beetle-induced tree mortality, to what degree does microbial functioning shift and are changes in microbial community structure correlated with shifts in function?

RESULTS

Edaphic properties. Soils of infested and dead clusters (groups of two to eight trees representing the same infestation stage) significantly differed from those of healthy clusters ($P < 0.05$; Fig. 1 and Table 1). Replicate samples taken within one cluster were treated as independent due to the fact that variation in edaphic conditions within a single cluster was greater than the expected measurement error. Thus, we did not want to mask the importance of edaphic conditions on community structure (20, 21). The soil environment in healthy clusters is characterized by a more acidic pH, lower electrical conductivity (EC), lower water content, lower percent weight C and N, and a lower C/N ratio (C:N) than the infested and dead clusters (Table 1). Both C and N concentrations increased as infestation stage progressed, but total carbon increased more rapidly than

TABLE 1 Edaphic properties of bulk soil in each infestation stage

	Mean ± SD[a]					
Infestation stage	pH	EC (μS/cm)	Water content (g/g [dry soil])	% wt, carbon (C)	% wt, nitrogen (N)	C:N
Healthy	4.84 ± 0.32^{A}	132.15 ± 43.78^{A}	0.26 ± 0.06^{A}	7.61 ± 2.55^{A}	0.40 ± 0.14^{A}	19.26 ± 3.32^{A}
Infested	5.21 ± 0.49^{B}	201.4 ± 72.17^{B}	0.47 ± 0.23^{B}	12.77 ± 7.13^{B}	0.58± 0.31^{B}	23.28 ± 4.22^{B}
Dead	5.17 ± 0.37^{B}	242.3 ± 80.0^{B}	1.06 ± 0.54^{C}	18.46 ± 10.69^{B}	0.83 ± 0.41^{B}	22.99 ± 4.78^{B}

[a]Different superscript letters indicate significant differences between infestation stages at $\alpha = 0.05$ as determined by Tukey's HSD test.

total nitrogen, which lead to the increased C:N ratio observed in infested and dead clusters.

Fungal diversity. Soil samples had an average of 106,175 reads ascribed to fungi per sample prior to processing, and an average of 61,995 reads were left (58.3% retention) after quality filtering and chimera removal. The remaining reads were clustered into a total of 3,157 amplicon sequence variants (ASVs), and after rarefaction 3,058 ASVs remained. When necessary the ASV table was rarefied to 14,749 reads per sample; the minimum number of reads for any sample which was successfully sequenced. We included 59 independent fungal samples in our analysis for both bulk and rhizosphere soils (missing one sample from dead cluster, due to unsuccessful amplification or sequencing).

In bulk soil, healthy clusters had both the lowest richness and Shannon diversity compared to dead and infested clusters ($P < 0.05$, Fig. 2). Dead clusters had the highest richness, and infested and dead clusters had higher Shannon diversity than the healthy clusters ($P < 0.05$). In rhizosphere soils, the same trends existed for richness and Shannon diversity, except no significant difference in richness was found between dead and infested clusters (Fig. 2). Beta diversity based on Bray-Curtis dissimilarities revealed significant differences between infestation stages ($F_{2,115} = 4.84$, $P < 0.001$, $R^2 = 0.0777$) and sampling time ($F_{1,116} = 1.53$, $P < 0.01$, $R^2 = 0.013$), but not soil origin ($F_{1,116} = 1.22$,

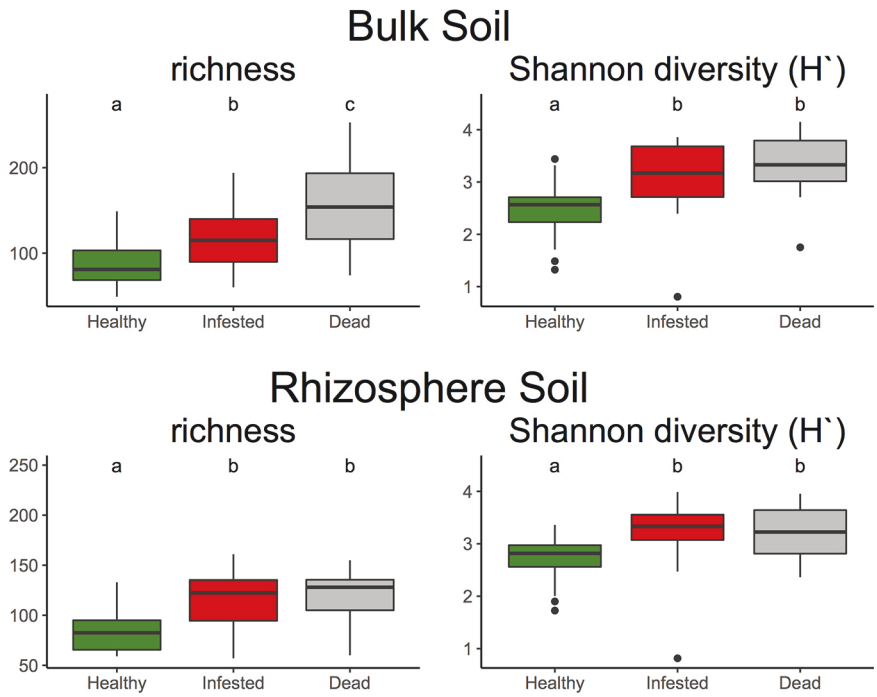

FIG 2 Fungal alpha-diversity metrics for bulk and rhizosphere soil. Line in boxes represent median, with top and bottom of boxes representing the 75th and 25th quartiles, respectively, and whiskers represent 1.5 × the interquartile range (IQR). Different letters indicate significant differences between infestation stages at $\alpha = 0.05$.

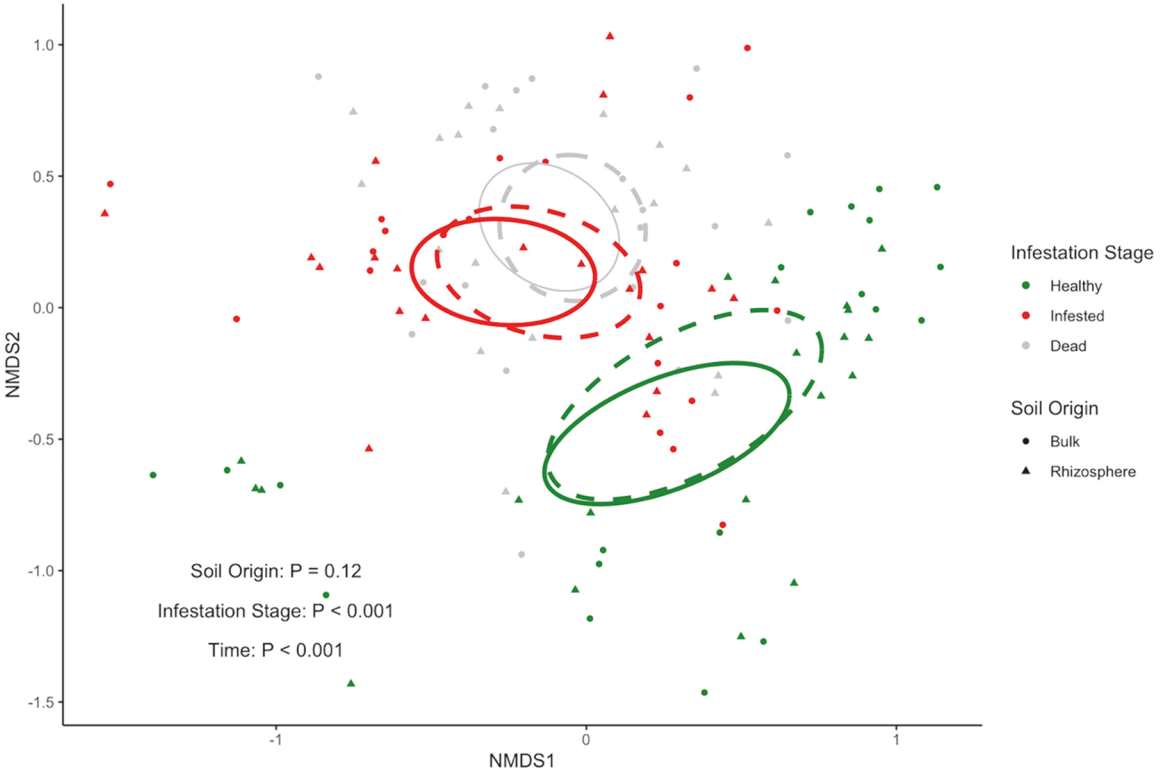

FIG 3 Nonmetric multidimensional scaling of fungal community based on Bray-Curtis dissimilarities, with community structure significantly different between infestation stages ($P < 0.001$) and time ($P < 0.01$), but not soil origin ($P = 0.12$) based on adonis testing. Ellipses represent the 95% confidence interval of the mean for each treatment type (soil origin and infestation stage). Dashed lines represent bulk soil, and solid lines represent rhizosphere soil. Points represent individual soil cores and are colored by infestation stage and shape indicates soil origin.

$P = 0.12$, $R^2 = 0.010$) (Fig. 3). Sampling time remained a significant explanatory variable for fungal community structure when the two sites sampled at a single time point were removed from the data set. Pairwise adonis testing with Bonferroni corrections indicated the bulk and rhizosphere soils were not significantly different from each other within a single infestation stage. All other pairwise comparisons among infestation stages were statistically significant ($P < 0.05$, average $\pm$ the standard error [SE]: $R^2 = 0.0714 \pm 0.002$) (e.g., dead bulk soil was different from healthy bulk soil, etc.). Mantel testing of the fungal community with edaphic parameters and geographic distance produced significant positive correlations between fungal community and geographic distance (Mantel R statistic = 0.2767, $P < 0.001$), pH (Mantel R statistic = 0.195, $P < 0.001$), C:N ratio (Mantel R statistic = 0.1583, $P < 0.001$), and electrical conductivity (Mantel R statistic = 0.1161, $P < 0.001$). Spearman's rho revealed significant correlations between species richness and total C ($\rho = 0.42$, $P < 0.001$), and total N ($\rho = 0.37$, $P < 0.01$). All correlations between Shannon diversity and total C and N, as well as the C:N, were positive and significant ($\rho > 0.335$, $P < 0.05$).

The majority of fungal taxa belonged to the Ascomycota and Basidiomycota phyla, with significant differences in the relative abundance of fungal phyla between infestation stages, and similar trends in both rhizosphere and bulk soil (Table 2). Of particular interest was the shift from roughly even abundances of basidiomycetes and ascomycetes to dominance of ascomycetes following infestation, which was caused by a higher relative abundance of all types of pathotrophs and saprotrophs in infested and dead compared to healthy clusters. In addition, symbiotrophs in the rhizosphere were significantly lower in the dead compared to healthy clusters (Table 2). Examination of taxa assigned specifically to ectomycorrhizae (ECM) by FUNGuild revealed the same significant trend, since the ECM represented the majority of symbiotrophs (Table 2). A

TABLE 2 Fungal phylum and trophic-mode abundances by infestation stage and soil origin[a]

	Mean ± SE[b]					
	Bulk			Rhizosphere		
Abundance type and organism	Healthy	Infested	Dead	Healthy	Infested	Dead
Phylum proportional abundances						
Ascomycota	0.55 ± 0.07^{A}	0.72 ± 0.05^{B}	0.73 ± 0.04^{B}	0.48 ± 0.06^{A}	0.69 ± 0.05^{B}	0.65 ± 0.07^{B}
Basidiomycota	0.45 ± 0.07^{A}	0.26 ± 0.05^{B}	0.21 ± 0.04^{B}	0.52 ± 0.06^{A}	0.20 ± 0.05^{B}	0.30 ± 0.06^{B}
Mortierellomycota	0.00 ± 0.00^{A}	0.02 ± 0.00^{B}	0.04 ± 0.01^{B}	0.00 ± 0.00^{A}	0.01 ± 0.00^{B}	0.02 ± 0.01^{B}
Mucoromycota	0.00 ± 0.00^{A}	0.00 ± 0.00^{A}	0.01 ± 0.01^{B}	0.00 ± 0.00^{A}	0.00 ± 0.00^{AB}	0.03 ± 0.02^{B}
Trophic-mode rarefied abundances						
Unknown	1,802.1 ± 510.01	2,554.15 ± 490.09	1,686.42 ± 202.41	589.85 ± 90.32^{A}	1,142.85 ± 205.32^{B}	1,754.0 ± 213.74^{B}
Pathotroph	49.65 ± 7.23^{A}	150.45 ± 29.20^{B}	160 ± 27.52^{B}	284.85 ± 49.35^{A}	516.2 ± 95.93^{B}	577.11 ± 90.36^{B}
Pathosaprotroph	61.85 ± 13.19^{A}	174.35 ± 35.69^{B}	477.95 ± 196.14^{C}	138.25 ± 41.25^{A}	436.75 ± 95.45^{B}	1,178.21 ± 270.03^{C}
Pathosymbiosaprotroph	1,598.30 ± 591.76^{A}	525.80 ± 121.07^{B}	568.63 ± 145.75^{B}	1,346.90 ± 535.95^{A}	408.40 ± 86.10^{B}	355.95 ± 116.14^{B}
Pathosymbiotroph	473.40 ± 105.92^{A}	1,150.80 ± 183.57^{B}	1,697.84 ± 427.55^{B}	413.65 ± 95.45^{A}	1,106.75 ± 177.95^{B}	1,014.05 ± 276.81^{B}
Saprotroph	1,693.85 ± 531.67	2,046.4 ± 658.37	2,147.21 ± 216.30	1,106.5 ± 286.67^{A}	2,373.1 ± 677.17^{B}	1,940.42 ± 389.82^{B}
Saprosymbiotroph	1,459.15 ± 360.00	1,328.90 ± 323.57	1,340.16 ± 236.33	901.60 ± 255.62	672.55 ± 129.34	781.53 ± 157.71
Symbiotroph	7,602.35 ± 673.76	6,818.15 ± 577.50	6,665.84 ± 660.86	9,967.4 ± 646.72^{A}	8,091.8 ± 645.06^{AB}	7,147.37 ± 709.93^{B}
Ectomycorrhizae	7,250.05 ± 648.19	6,035.6 ± 531.10	6,399.26 ± 663.78	9,425.05 ± 616.40^{A}	7,382.25 ± 611.61^{AB}	6,549.63 ± 728.20^{B}

[a]Phylum abundances are reported as within sample proportional abundances. Only phyla with a >1% mean relative abundance in at least one infestation stage are reported. Trophic-mode abundances are reported as rarefied counts due to the fact that only rarefied counts were used for those analyses. Trophic modes with at least 500 counts in at least one treatment are reported. Ectomycorrhizae are the only guild reported due to their ecological importance.

[b]Different superscript letters indicate significant differences between infestation stages at $\alpha = 0.05$ as determined by Tukey's HSD test and are soil origin specific. A lack of letters indicates no significant differences between infestation stages.

TABLE 3 Differentially abundant fungal taxa at the genus level ($P < 0.05$), based on DESeq2 analysis, and associated FUNGuild assignments to guild, between healthy and dead clusters and associated guild assignment[a]

Soil origin and associated infestation stage	Mean relative abundance	Change (log_2 fold)	Adjusted *P* value	Family	Genus	Guild as assigned by FUNGuild
Bulk						
Healthy	9.58	−23.79	0.001	*Hymenogastraceae*	*Hebeloma*	Ectomycorrhizal
	17.46	−8.04	0.001	*Boletaceae*	*Boletus*	Ectomycorrhizal
	404.74	−7.97	0.017	*Rickenellaceae*	*Alloclavaria*	Undefined saprotroph: hypothesized ectomycorrhizae
	4.82	−5.87	0.027	*Thelephoraceae*	*Tomentellopsis*	Ectomycorrhizal
	1,043.3	−4.29	0.001	*Cortinariaceae*	*Cortinarius*	Ectomycorrhizal
	235.97	−2.09	0.014	*Helotiaceae*	*Meliniomyces*	Ectomycorrhizal-endophyte-ericoid mycorrhizal-litter saprotroph-orchid mycorrhizal
	704.86	−2.05	0.044	*Pyronemataceae*	*Trichophaea*	Dung saprotroph-ectomycorrhizal
	2,225.93	−1.83	0.029	*Atheliaceae*	*Amphinema*	Ectomycorrhizal
Dead	187.26	2.15	0.001	*Mortierellaceae*	*Mortierella*	Endophyte-litter saprotroph-soil saprotroph-undefined saprotroph
	69.57	2.65	0.001	*Umbelopsidaceae*	*Umbelopsis*	Undefined saprotroph
	52.82	2.98	0.017	*Herpotrichiellaceae*	*Cladophialophora*	Undefined saprotroph
	2.9	3.39	0.034	*Tricholomataceae*	*Fayodia*	Undefined saprotroph
	2.99	3.77	0.017	*Leucosporidiaceae*	*Mastigobasidium*	
	3.97	3.99	0.029	*Gautieriaceae*	*Gautieria*	Ectomycorrhizal
	55.45	4.4	0.001	*Helotiales_fam_Incertae_sedis*	*Xenopolyscytalum*	Undefined saprotroph
	4.16	4.73	0.006	*Hysterangiaceae*	*Hysterangium*	Ectomycorrhizal
	7.47	4.98	0.014	*Psathyrellaceae*	*Parasola*	Undefined saprotroph
	4.68	5.22	0.001	*Dermateaceae*	*Pezicula*	Endophyte-plant pathogen-undefined saprotroph
	251.61	8.63	0.001	*Pyronemataceae*	*Geopora*	Ectomycorrhizal
Rhizosphere						
Healthy	52.46	−9.43	0.001	*Boletaceae*	*Boletus*	Ectomycorrhizal
	11.48	−5.78	0.012	*Hypocreaceae*	*Hypomyces*	Undefined saprotroph
	109.38	−3.65	0.014	*Coniochaetaceae*	*Lecythophora*	Endophyte
	442.87	−3.49	0.004	*Cortinariaceae*	*Cortinarius*	
	1,058.87	−2.64	0.046	*Atheliaceae*	*Piloderma*	Ectomycorrhizal
Dead	217.61	1.81	0.004	*Vibrisseaceae*	*Phialocephala*	Endophyte
	436.25	3.03	0.003	*Tricholomataceae*	*Mycena*	Ectomycorrhizal-fungal parasite
	100.73	3.76	0.001	*Helotiales_fam_Incertae_sedis*	*Xenopolyscytalum*	Undefined saprotroph
	36.84	7.66	0.001	*Dermateaceae*	*Pezicula*	Endophyte-plant pathogen-undefined saprotroph
	416.83	9.54	0.001	*Pyronemataceae*	*Geopora*	Ectomycorrhizal

[a]Associations are marked by both soil origin and infestation stage. Taxon order is determined by the value of the log_2 change within each soil origin. The mean relative abundance represents rarefied taxon abundance across all samples. The change column (log_2 fold) represents the multiplicative change in taxon abundance from healthy to dead clusters. Negative numbers represent a trend of decreasing abundance as infestation progressed; thus, higher relative abundances in healthy clusters. Positive numbers represent an increase in relative abundance as infestation progressed; thus, higher abundances in dead clusters. The adjusted *P* value reflects the *P* value after FDR multiple-comparison correction.

separate analysis of ECM alpha-diversity revealed significantly lower richness in bulk soil of healthy compared to infested clusters ($P < 0.05$), but dead clusters were not significantly different from healthy or infested clusters. Infested clusters had the highest ECM richness in bulk soils. No significant differences in ECM Shannon diversity were found among infestation stages for bulk soils. In rhizosphere soils, infested clusters had the highest ECM Shannon diversity and was higher compared to dead clusters ($P < 0.05$). However, healthy clusters were not different from either infested or dead clusters. No differences in ECM richness were found among infestation stages in rhizosphere soils.

Differential abundance analysis, using DESeq2, revealed 24 taxa to be differentially abundant at the genus level ($P < 0.05$), 14 of which were associated with bulk soil, 5 were associated with rhizosphere soil, and 5 were found in both bulk and rhizosphere (Table 3). In rhizosphere soil, five taxa were associated with healthy clusters and five with dead clusters. FUNGuild assigned three of the five healthy cluster rhizosphere taxa as symbionts (two ectomycorrhizal and one endophytic). In dead clusters, there was a

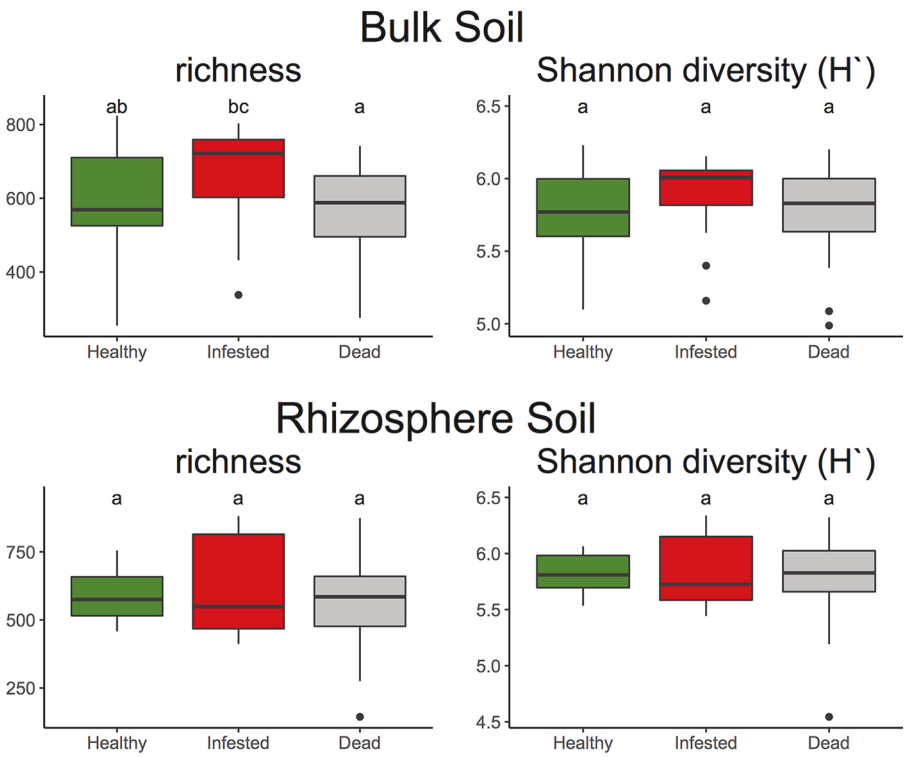

FIG 4 Bacterial alpha-diversity metrics for bulk and rhizosphere soil. Lines in boxes represent medians, with tops and bottoms of boxes representing the 75th and 25th quartiles, respectively, and whiskers represent 1.5 × IQR. Different letters indicate significant differences between infestation stages at $\alpha = 0.05$.

mixture of symbionts and pathogens; two symbionts (one ectomycorrhizal and one endophytic taxon) and three taxa defined as pathogenic or saprotrophic. In bulk soils, eight taxa were associated with healthy clusters and eleven with dead clusters. Significant taxa of healthy cluster bulk soil were overwhelmingly ectomycorrhizal (seven of the eight). In dead clusters, the majority of taxa were assigned to a saprotrophic guild (seven of the eleven). In addition, three ectomycorrhizal taxa were indicators of bulk soil in dead clusters.

Bacterial diversity. Soil samples had an average of 58,565 reads ascribed to bacteria per sample prior to processing, and after quality filtering and chimera removal an average of 45,810 reads were left (78% retention). A total of 16,271 unique ASVs were assigned, and 9,736 unique ASVs remained after rarefaction. When necessary the ASV table was rarefied to 2,148 reads per sample; the minimum number of reads for any sample which was successfully sequenced. We included 19 healthy, 18 infested, and 19 dead independent bulk soil samples and 19 healthy, 15 infested, and 19 dead independent rhizosphere soil samples in our analysis. The final number of samples differs from the number collected due to unsuccessful amplification or sequencing.

Bacterial richness in the bulk soil was higher in infested compared to dead clusters ($P < 0.05$), and marginally higher compared to healthy clusters ($P < 0.1$) (Fig. 4). No significant differences in alpha-diversity were found for rhizosphere soils. Bacterial community structure, based on Bray-Curtis analysis, was significantly different among infestation stages ($F_{2,106} = 5.88$, $P < 0.001$, $R^2 = 0.10$) and soil origin ($F_{1,107} = 4.85$, $P < 0.001$, $R^2 = 0.043$) (Fig. 5). Sampling time was marginally significant ($F_{1,107} = 1.54$, $P = 0.057$, $R^2 = 0.014$). Pairwise adonis testing with Bonferroni corrections for multiple comparisons indicated that healthy clusters had a significant difference in bacterial community structure between bulk and rhizosphere soil ($F_{1,107} = 3.59$, $P < 0.05$, $R^2 = 0.09$), but this was not the case for the infested and dead clusters ($P > 0.1$, $R^2 = 0.058$. Fig. 5). In addition, the rhizosphere bacterial communities of dead and infested clusters

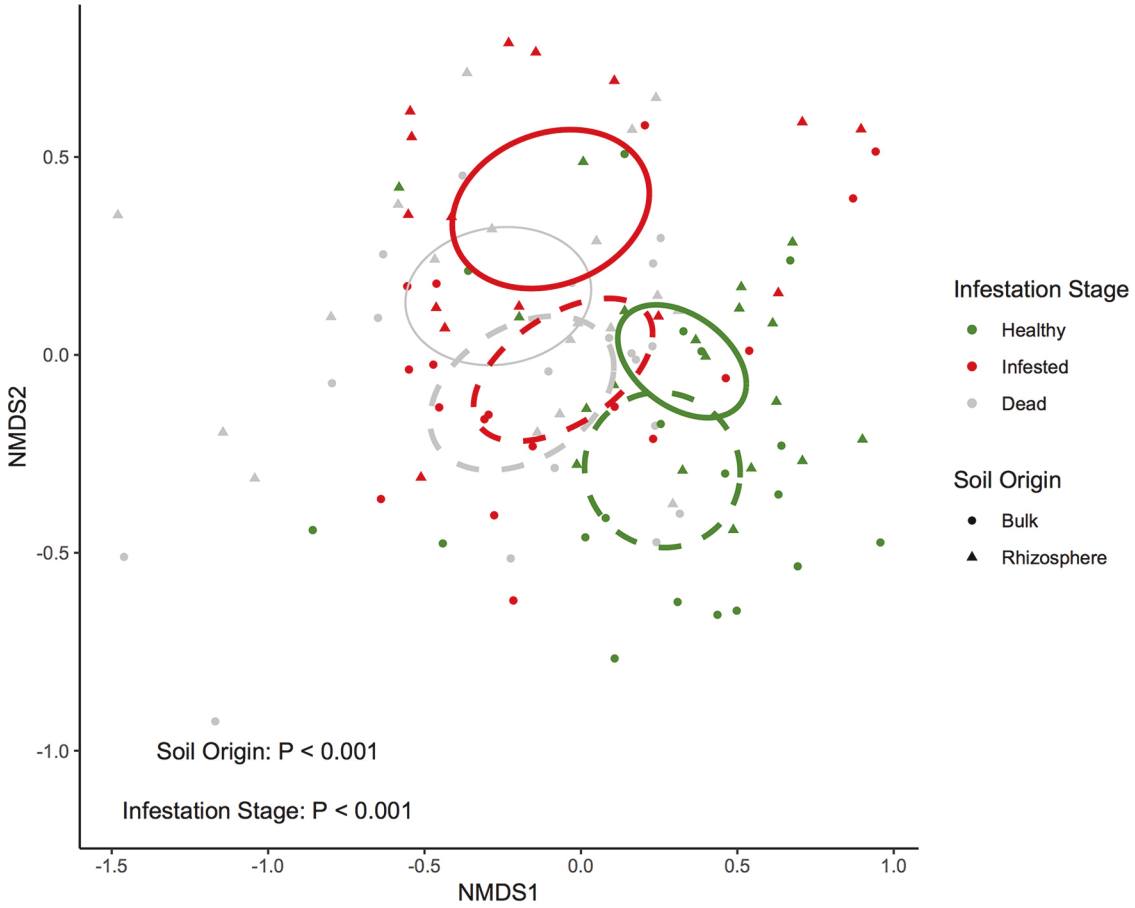

FIG 5 NMDS of bacterial community based on Bray-Curtis dissimilarities, with community structure significantly different between infestation stages ($P < 0.001$) and soil origin ($P < 0.001$) based on adonis testing. Ellipses represent the 95% confidence interval for the mean for each treatment type (soil origin and infestation stage). Dashed lines represent bulk soil, and solid lines represent rhizosphere soil. Points represent individual soil cores and are colored by infestation stage, and the shape indicates soil origin.

were not statistically different from each other, but both were different from the healthy cluster rhizosphere ($P < 0.05$, $R^2 = 0.12$).

Mantel testing of the bacterial community with edaphic parameters and geographic distance produced significant correlations between bacterial community and both C:N ratio (Mantel R statistic = 0.5636, $P < 0.01$) and pH (Mantel R statistic = 0.4653, $P < 0.01$), which were similar to the results of the fungal community. In addition, fungal and bacterial community dissimilarities were significantly correlated for both bulk and rhizosphere soil (Mantel R statistic = 0.3715, $P < 0.01$, and Mantel R statistic = 0.3267, $P < 0.01$, respectively). Spearman's rho revealed no significant correlations between bacterial alpha-diversity metrics and total C, total N, or C:N.

Of the ten phyla observed, the proteobacteria were most abundant in both bulk and rhizosphere soils (Table 4). Several bacterial phyla had significant differences in relative abundance among infestation stages: seven phyla in the bulk soil (*Verrucomicrobia*, *Acidobacteria*, *Bacteroidetes*, *Firmicutes*, *Chloroflexi*, *Gemmatimonadetes*, and *Armatimonadetes*) and four in the rhizosphere soil (*Acidobacteria*, *Bacteroidetes*, *Chloroflexi*, and *Armatimonadetes*) (Table 4). Differential abundance analysis via DESeq2 revealed 16 taxa at the genus level to be associated with healthy clusters and bulk soil, eight associated with rhizosphere soils, and eight were associated with both bulk and rhizosphere soils (Table 5). In the dead clusters, a total of 18 unique taxa were deemed significant, nine in rhizosphere soils, five in bulk, and four were shared between both bulk and rhizosphere soils (Table 5).

TABLE 4 Bacterial phylum abundances by infestation stage and soil origin[a]

	Mean ± SE[b]					
	Bulk			Rhizosphere		
Phylum	Healthy	Infested	Dead	Healthy	Infested	Dead
Proteobacteria	0.24 ± 0.01	0.27 ± 0.01	0.26 ± 0.01	0.31 ± 0.01	0.33 ± 0.01	0.31 ± 0.01
Verrucomicrobia	0.14 ± 0.01^{A}	0.19 ± 0.01^{B}	0.17 ± 0.01^{AB}	0.13 ± 0.01	0.15 ± 0.01	0.14 ± 0.01
Acidobacteria	0.19 ± 0.01^{A}	0.16 ± 0.01^{AB}	0.15 ± 0.01^{B}	0.15 ± 0.00^{A}	0.13 ± 0.01^{AB}	0.13 ± 0.01^{A}
Actinobacteria	0.11 ± 0.01	0.11 ± 0.01	0.13 ± 0.02	0.13 ± 0.01	0.17 ± 0.02	0.15 ± 0.01
Bacteroidetes	0.05 ± 0.01^{A}	0.05 ± 0.01^{A}	0.08 ± 0.01^{B}	0.04 ± 0.00^{A}	0.06 ± 0.00^{B}	0.06 ± 0.00^{B}
Planctomycetes	0.12 ± 0.01	0.13 ± 0.00	0.13 ± 0.01	0.13 ± 0.01	0.11 ± 0.01	0.13 ± 0.01
Firmicutes	0.02 ± 0.00^{A}	0.01 ± 0.00^{B}	0.01 ± 0.00^{B}	0.01 ± 0.00	0.01 ± 0.00	0.01 ± 0.00
Chloroflexi	0.09 ± 0.01^{A}	0.05 ± 0.01^{B}	0.04 ± 0.01^{B}	0.06 ± 0.01^{A}	0.02 ± 0.00^{B}	0.04 ± 0.00^{C}
Gemmatimonadetes	0.02 ± 0.00^{A}	0.01 ± 0.00^{B}	0.01 ± 0.00^{B}	0.01 ± 0.00	0.01 ± 0.00	0.01 ± 0.00
Armatimonadetes	0.01 ± 0.00^{A}	0.01 ± 0.00^{B}	0.01 ± 0.00^{AB}	0.01 ± 0.00^{A}	0.01 ± 0.00^{B}	0.01 ± 0.00^{B}

[a]Phylum abundances are reported as within in sample proportional abundances. Only phyla with > 1% mean relative abundance in at least one infestation stage are reported.

[b]Different superscript letters indicate significant differences between infestation stages at $\alpha = 0.05$ as determined by Tukey's HSD test and are soil origin specific. A lack of letters indicates no significant differences between infestation stages.

Extracellular enzyme activities. Three carbon (β-glucosidase [BG], α-glucosidase [AG], and cellobiohydrolase [CBH]) and one nitrogen (leucine aminopeptidase [LAP]) cycling enzymes had significantly higher enzyme activities in dead clusters compared to healthy and infested clusters ($P < 0.05$) (Fig. 6). The nitrogen cycling enzyme *N*-acetyl-β-glucosaminidase (NAG) showed a significant increase following infestation ($P < 0.05$) and remained high in the dead clusters (Fig. 6). Acid phosphatase (PHOS) was significantly higher in dead clusters compared to healthy but not infested clusters ($P < 0.05$) (Fig. 6). Both lignin-degrading enzymes, peroxidases (PEROX) and phenol oxidase (PHENOX), had the highest activities in infested clusters ($P < 0.05$) (Fig. 6). Pairwise adonis testing with Bonferroni corrections for multiple comparisons indicated enzyme profiles of healthy and dead clusters to be significantly different from each other ($F_{2,50} = 6.85$, $P < 0.05$, $R^2 = 0.18$). Neither were significantly different from infested clusters.

Mantel testing revealed that enzyme activities were most strongly correlated with gravimetric water content (Mantel R statistic = 0.6645, $P < 0.001$), followed by fungal community (Mantel R statistic = 0.2107, $P < 0.05$), bacterial community (Mantel R statistic = 0.144, $P < 0.05$), electrical conductivity (Mantel R statistic = 0.1063, $P < 0.05$), and also marginally correlated to the C:N ratio (Mantel R statistic = 0.1424, $P = 0.077$). Spearman's rho showed significant positive relationships ($\rho > 0.24$, $P < 0.05$) between the following: (i) total enzymatic activity and %C, %N, and C:N; (ii) total hydrolytic C enzyme activity (BG + CBH + BX + AG) and %C, %N, and C:N; and (iii) total N enzyme activity (NAG + LAP) and %C, %N, and C:N. The ratio of hydrolytic C enzymes to N enzymes and soil C:N showed a negative relationship ($\rho = -0.33$, $P < 0.05$). No significant correlations were found for lignolytic enzymes and %C, %N, or C:N.

DISCUSSION

It is well documented that bark beetle infestation affects the soil environment (5, 6, 9, 14, 22), and our survey supports these previous findings. Increased soil moisture in dead clusters is likely a product of decreased evapotranspiration. The shift toward a more neutral pH in the infested and dead clusters was likely driven by the cessation of rhizodeposits following beetle kill since they contain organic acids and can leach from the rhizosphere into the bulk soil, lowering the pH. In addition to rhizodeposits, live trees take up cations from the soil such as Ca^{2+} and Mg^{2+}, which leads to increased binding sites for H^{+}, resulting in a more acidic pH in the live clusters compared to dead and infested (23). The lower EC values in the healthy clusters are likely driven by the same process of cation uptake. Once trees are no longer utilizing these nutrients, they are able to accumulate in soil, increasing the EC.

Our expectation, based on previous work (14, 24), was that we would find the lowest

TABLE 5 Differentially abundant bacterial taxa at the genus level ($P < 0.05$) based on DESeq2 analysis between healthy and dead clusters[a]

Soil origin and associated infestation stage	Mean relative abundance	Change (log_2 fold)	Adjusted *P* value	Family	Genus
Bulk					
Healthy	1.65	−3.02	0.009	*Catenulisporaceae*	*Catenulispora*
	5.59	−2.61	0.005	*Ktedonobacteraceae*	*Ktedonobacter*
	5.85	−2.33	0.007	*Acidobacteriaceae*_(subgroup_1)	*Candidatus* Koribacter
	4.73	−2.29	0.003	*Acidobacteriaceae*_(subgroup_1)	*Occallatibacter*
	5.54	−1.78	0.045	*Acidobacteriaceae*_(subgroup_1)	*Acidobacterium*
	8.55	−1.09	0.047	*Burkholderiaceae*	*Burkholderia-Paraburkholderia*
	37.84	−0.97	0.028	*Acidothermaceae*	*Acidothermus*
	10.41	−0.90	0.025	*Chthonomonadaceae*	*Chthonomonas*
Dead	12.13	1.07	0.013	*Rhodospirillales_Incertae_Sedis*	*Reyranella*
	11.85	1.21	0.005	*Opitutaceae*	*Opitutus*
	16.05	1.29	0.005	*Planctomycetaceae*	Pir4_lineage
	3.95	1.66	0.021	*Hyphomicrobiaceae*	*Devosia*
	2.80	2.19	0.028	*Verrucomicrobiaceae*	*Luteolibacter*
	1.33	2.42	0.026	*Chitinophagaceae*	*Parafilimonas*
	2.47	2.48	0.008	*Chitinophagaceae*	*Terrimonas*
	1.60	2.56	0.025	*Phaselicystidaceae*	*Phaselicystis*
	9.17	3.60	0.005	*Streptomycetaceae*	*Streptomyces*
Rhizosphere					
Healthy	6.07	−3.94	0.000	Acidobacteriaceae_(subgroup_1)	*Candidatus* Koribacter
	2.76	−3.48	0.021	*Geobacteraceae*	*Geobacter*
	1.29	−3.20	0.019	*Bradyrhizobiaceae*	*Rhodoblastus*
	4.05	−2.83	0.003	*Catenulisporaceae*	*Catenulispora*
	0.96	−2.72	0.014	*Rhodospirillaceae*	*Skermanella*
	6.91	−2.33	0.001	*Acidobacteriaceae*_(subgroup_1)	*Occallatibacter*
	3.46	−2.00	0.021	*Ktedonobacteraceae*	*Ktedonobacter*
	5.33	−1.99	0.000	*Rhodospirillaceae*	*Inquilinus*
	13.90	−1.70	0.000	*Chthonomonadaceae*	*Chthonomonas*
	15.78	−1.39	0.000	*Burkholderiaceae*	*Burkholderia-Paraburkholderia*
	12.89	−1.36	0.021	*Acidobacteriaceae*_(subgroup_1)	*Acidobacterium*
	24.14	−1.24	0.000	*Solibacteraceae*_(subgroup_3)	*Candidatus* Solibacter
	43.59	−1.08	0.010	*Acidothermaceae*	*Acidothermus*
	29.70	−1.05	0.014	*Acidobacteriaceae*_(subgroup_1)	*Granulicella*
	13.88	−0.83	0.014	*Caulobacteraceae*	*Phenylobacterium*
	14.29	−0.67	0.050	*Solibacteraceae*_(subgroup_3)	*Bryobacter*
Dead	9.40	1.14	0.001	*opitutaceae*	*Opitutus*
	5.87	1.29	0.037	*Hyphomicrobiaceae*	*Devosia*
	15.86	1.47	0.005	*Planctomycetaceae*	Pir4_lineage
	3.09	1.60	0.026	*Planctomycetaceae*	*Pirellula*
	3.15	1.90	0.039	*Solirubrobacteraceae*	*Solirubrobacter*
	1.68	2.08	0.021	*Chthoniobacterales_Incertae_Sedis*	*Terrimicrobium*
	8.64	2.27	0.001	*Flavobacteriaceae*	*Flavobacterium*
	1.70	2.29	0.032	*Chitinophagaceae*	*Terrimonas*
	3.13	2.36	0.014	*Xanthomonadaceae*	*Arenimonas*
	4.54	2.69	0.000	*Cryptosporangiaceae*	*Cryptosporangium*
	0.90	2.94	0.014	*Cellvibrionaceae*	*Cellvibrio*
	0.99	3.13	0.019	*Caulobacteraceae*	*Caulobacter*
	1.00	3.34	0.014	*Nitrosomonadaceae*	*Nitrosospira*

[a]Associations are marked by both soil origin and infestation stage. Taxon order is determined by value of log_2 change within each soil origin. The mean relative abundance represents the rarefied taxon abundance across all samples. The change column (log_2 fold) represents the multiplicative change in in taxon abundance from healthy to dead clusters. Negative numbers represent a trend of decreasing abundance as infestation progressed; thus, higher relative abundances in healthy clusters. Positive numbers represent an increase in relative abundance as infestation progressed; thus, higher abundances in dead clusters. The adjusted *P* value reflects the *P* value after FDR multiple-comparison correction.

soil C:N ratio in the infested and dead clusters following decomposition of N-rich needles deposited from the dying trees. We expected increased rates of decomposition in the infested and dead clusters since decreased canopy cover could allow for increased solar radiation and precipitation reaching the forest floor. However, our results showed that while total N increased in dead and infested clusters, similar to other studies, total C did at a higher rate, leading to the observed increase in C:N ratio. The observed increase in soil carbon may a product of C from partially decomposed

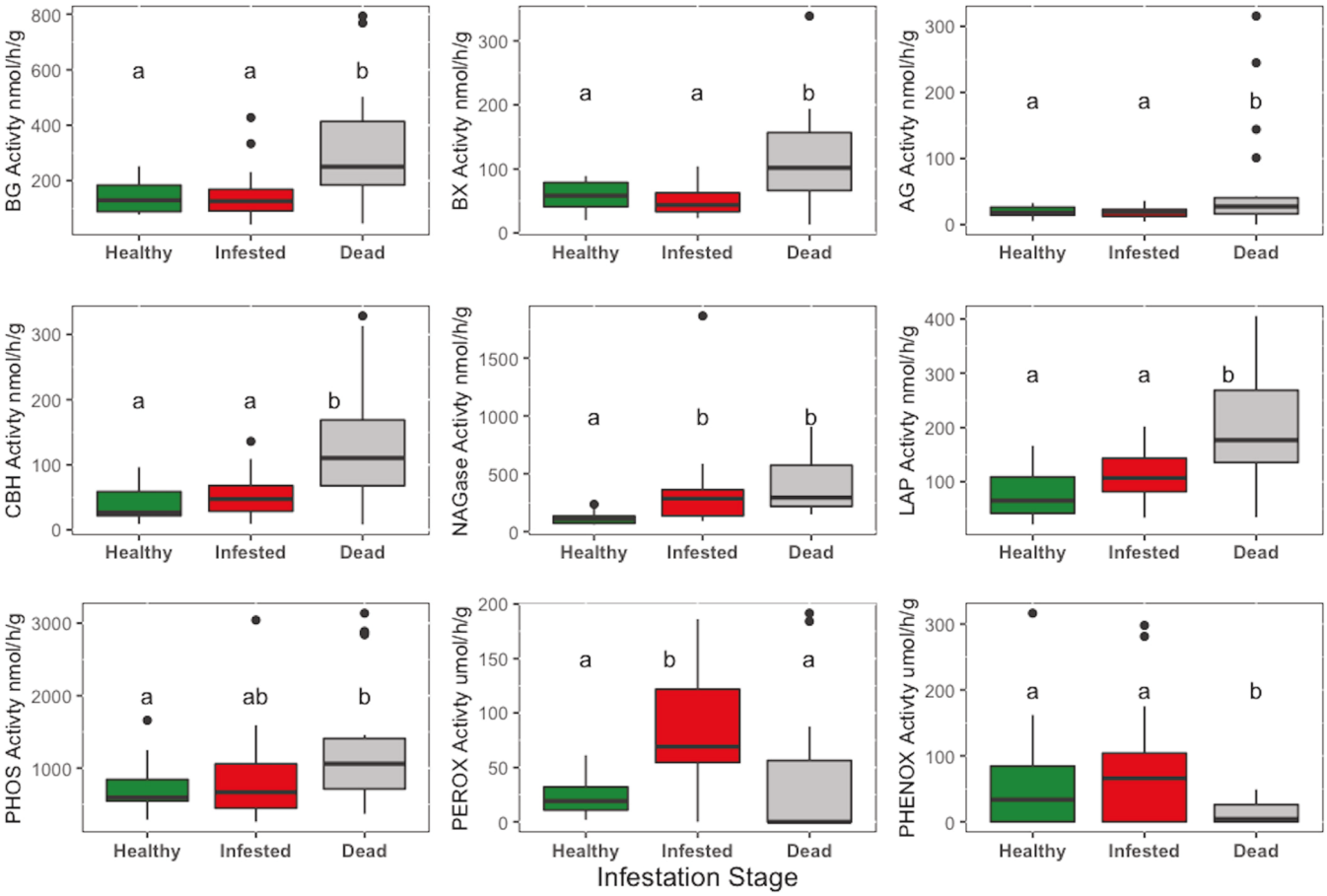

FIG 6 Soil extracellular enzyme activities in the different infestation stages for β-glucosidase (BG), β-xylosidase (BX), α-glucosidase (AG), cellobiohydrolase (CBH), *N*-acetyl-β-glucosaminidase (NAG), leucine aminopeptidase (LAP), acid phosphatase (PHOS), gross peroxidases (PEROX), and phenol oxidase (PHENOX). Different letters indicate significant differences between infestation stages for each enzyme at $\alpha = 0.05$.

needles combined with increased microbial biomass C. As carbon is required in larger amounts than nitrogen for microbial metabolism, increases in microbial biomass would accumulate carbon more quickly than nitrogen, explaining our higher soil C:N ratio. Another possible explanation for the increased C:N ratio in infested and dead clusters could be partial removal of N by exploratory ECM associated with nearby living trees, i.e., ECM mine N from organic matter (25) in the dead and infested clusters and provide it to their host trees in nearby healthy clusters. Furthermore, Bödeker et al. (26) showed that some ectomycorrhiza produce Mn peroxidase enzymes capable of degrading lignin and removing N from the humus layer in northern forest ecosystems, thus providing more support that mycorrhizal taxa contribute to nitrogen mobilization. These theories are in line with the observed increased N-cycling enzyme activities in infested and dead clusters and disproportionate increase in soil C and soil N.

In addition to the observed physicochemical changes in the soil environment, beetle infestation also resulted in significantly different fungal and bacterial communities. Each kingdom responded in a unique manner, with each expressing different trends in alpha- and beta-diversities across infestation stages and soil origins. Differences in relative abundance of fungal and bacterial phyla suggest a restructuring of the microbial community following bark beetle infestation, observable even at coarse taxonomic resolution. Significant increases in fungal richness as infestation progressed suggest open niche space allowing other taxa to become established, likely a result of the changes in availability and diversity of substrates through inputs of litter and dead root biomass and reduction in rhizodeposits (24). This finding is at odds with Hopkins et al.

(19), who reported no changes in fungal richness in the rhizosphere, suggesting the response of rhizosphere microbes to host mortality may be host and/or ecosystem specific. Furthermore, the change from rhizodeposits to more recalcitrant organic molecules from litter and root necromass could allow taxa which were once outcompeted by copiotrophs to proliferate. This hypothesis is supported by the increased NAG activity observed in infested and dead clusters. NAG is involved in chitin degradation and, as such, a proxy for fungal biomass turnover. Infestation stages showed no significant pairwise differences in fungal community structure between rhizosphere and bulk soil, likely a result of the growth morphology of fungi. Fungi explore the soil environment via hyphal growth. Therefore, the same taxa present in rhizosphere may also be present in bulk soil. Mantel correlations between the fungal community, and edaphic parameters supports previous findings that pH, C:N ratio, and carbon substrates are important drivers of community assembly (27, 28).

While ectomycorrhizal fungi are best known for their symbiotic relationships with host plants, previous research has proposed ECM species to be potent decomposers and can contribute significantly to soil C and N cycling (26, 29–31). With this and the observed shifts in C:N ratios in mind, we formulated two possible explanations for ECM remaining in the system following bark beetle infestation at our sites. First, ECM could potentially become saprophytes in the absence of suitable host plants, which is partially supported by their known enzymatic abilities (26, 30, 31), specifically oxidative enzymes (26, 31), and *in vitro* experimentation showing ectomycorrhizal taxa to adopt a saprotrophic lifestyle (32) as is the case with many facultative saprophytic plant pathogens. In this case, the ECM would survive as free-living fungi. The spike in the lignolytic enzyme activity observed in infested clusters provides support for this shift in ECM lifestyle to facultative saprotrophs. However, this hypothesis remains controversial (29, 33) and is not widely accepted in the literature. A second possible explanation is that ECM found at our study sites remain symbiotic and are associated with nearby living trees. This coincides with our hypothesis explaining the increased C:N ratio found in infested and dead clusters. ECM hyphae radiate into the soil environment in search of nutrients, and infested and dead clusters provide an environment with available nutrients from needle drop and decaying roots. We lack information regarding exploration type of the majority of ECM taxa at our sites and this should be considered an avenue for future research, as should the enzymatic capabilities of individual ECM taxa. These gaps in knowledge limit our ability to discern the ecology behind the ECM response to disturbance. The hypothesis of ECM radiating from nearby clusters suggests that our study design did not completely isolate infestation stages, which is inherent to bark beetle infested forest; there is always some degree of patchiness in bark beetle-induced tree mortality. However, even with this patchiness, our results show that the indirect impacts of bark beetle-induced tree mortality on soil microbial function and diversity to be both biologically and statistically significant. While ECM radiating from nearby live stands could contribute to ECM community homogeneity between live and dead clusters, potentially masking shifts in biotic characteristics, our result still suggest a strong change in fungal characteristics following bark beetle-induced tree mortality.

Furthermore, differential abundance analysis (DESeq2) provides support for our hypothesis of decreased mutualists and increased saprotrophic and pathogenic taxa following infestation and coincides with previous work showing similar trends (10, 12). In healthy clusters, two of the five indicator taxa of rhizosphere soils were assigned as ectomycorrhizal taxa, while in dead clusters more indicator taxa were assigned to saprotrophs, and different ectomycorrhizal indicator taxa compared to the healthy clusters. In bulk soil, the same trends were observed, with almost all of the indicator taxa of the healthy cluster assigned to ectomycorrhizal and the last one, *Alloclavaria*, while assigned to a saprotrophic trophic mode, has been hypothesized to be mycorrhizal (34). Following infestation, the dramatic shift to saprotrophic and pathogenic indicator taxa (seven out of eleven) also supports the work of Šťursová et al. (10). As symbiotic taxa decline, open niche space allows saprotrophic and pathogenic taxa to

increase in proportional abundance and could contribute to observed differences in community structure and function, i.e., increased enzymatic activity. Our results suggest ectomycorrhizal taxa may be less competitive in an environment lacking suitable living hosts, but not to the point of local extinction, potentially explaining the hypotheses put forward in this discussion.

In the bacterial community, alpha- and beta-diversity trends were different from the fungal community. Though there was a trend of increased bacterial richness in the bulk soil of the infested clusters, it was not significant, and the rhizosphere soil had a stable number of taxa in all infestation stages. The lack of bark beetle-induced effects on soil bacterial alpha-diversity matches results from Mikkelson et al. (13) and Ferrenberg et al. (15). However, even though species richness was not affected, the bacterial community structure was significantly altered following bark beetle infestation, which is similar to results from the heavily impacted site in the study by Mikkelson et al. (13), but contrasts with the moderately impacted site of Mikkelson et al. (14), as well as the sites from Ferrenberg et al. (15). These contrasting results could be caused by differences in mortality levels and forest type, *Pinus* spp. versus *Picea engelmanii* in our study. We originally hypothesized that the rhizosphere community would be different from the bulk soil across infestation stages. However, we did not find this to be true and observed a convergence of the rhizosphere and bulk bacterial communities following infestation, while healthy clusters maintained distinct bulk and rhizosphere bacterial communities. This may be driven by the reliance of select bacteria on rhizodeposits (35, 36). Once rhizodeposition stops, the rhizosphere becomes less hospitable to bacteria only equipped to degrade simple compounds, or specific rhizosphere exudates, and becomes more like the bulk soil environment, resulting in bacterial community convergence. The rhizosphere of the dead clusters likely did not converge to the bulk soil in healthy clusters due to the continued input of root necromass. In addition, we found greater divergence in the rhizosphere communities than in bulk soil communities after infestation, suggesting the rhizosphere was impacted more than the bulk soil. This finding also supports the lack of significantly different soil bacterial communities at the Mikkelson et al. (13) and Ferrenberg et al. (15) study sites, which focused only on the bulk soil environment. Furthermore, unlike fungi, bacterial richness was not correlated with total C, total N, or C:N ratio, suggesting shifts in nutrient availability and substrate diversity do not significantly contribute to bacterial diversity as much as fungal diversity. Lauber et al. (37) reported the C:N ratio and the % organic carbon to be nonsignificant in bacterial diversity at a continental scale, and our results suggest this to be true at the local ecosystem scale as well. Differences in phylum level relative abundances suggest that bark beetle influences microbial community structure at coarse taxonomic resolution, a result similar to fungi.

The observed shifts in overall soil microbial community structure following bark beetle infestation coincide with changes in microbial functioning based on enzymatic activity profiles. The fungal community structure was more strongly correlated to enzymatic profiles than the bacterial community, indicating that the bark beetle-induced changes in the fungal community had a larger influence on changes in enzymatic activity profile. However, the stronger correlation between enzymatic profiles and the fungal community may be an artifact of the lower taxon richness in the fungal compared to the bacterial community, i.e., a change in one taxon in the fungal community could have a proportionally stronger effect compared to a change in one taxon in the more diverse bacterial community. The increased enzymatic activities following bark beetle-induced mortality demonstrates the importance of soil microbes and their involvement in nutrient cycling following spruce beetle infestation. Borkhuu et al. (32) reported soil respiration profiles to be constant following bark beetle infestation in lodgepole pine forests. These authors proposed this to be caused by increased soil heterotrophic respiration filling in for the absence of autotrophic respiration (root respiration) following beetle kill. This hypothesis is supported by the observed increase in enzymatic activities in our study, as well as the positive correlations between enzymatic activity and soil C and N, which were also found in other

studies (38, 39), and could be explained by an increase in the variety of substrates available to soil microbes (39).

In summary, our study demonstrated several impacts of bark beetle-induced tree mortality on the soil environment and shows that altered edaphic parameters, coupled with the absence of root exudates, select a different consortium of microbial taxa and result in altered microbial community structure and function. Bark beetle infestation was shown to affect bacterial and fungal communities in different manners, with soil origin being important for the bacterial community but not the fungal community. In both cases, phylum-level differences in abundance suggest that bark beetle infestation results in coarse restructuring of the soil microbial community. This shift in microbial community structure was associated with elevated enzymatic activities, suggesting increased activity and nutrient cycling by microbes. As expected, our results showed decreased abundance of symbiotic mycorrhizal taxa and increases in pathogenic and saprotrophic fungal taxa following bark beetle infestation, and these changes were most pronounced in the rhizosphere environment. Increases in C and N stocks coupled with increased enzymatic activity could have implications in seedling regeneration, as well as C and N sink-source dynamics. Future work needs to address mycorrhizal ecology following bark beetle infestation to determine what, if any, are the long-term impacts of bark beetle on forest regeneration.

MATERIALS AND METHODS

Site descriptions. Our study site was located in the Medicine Bow-Routt National Forest in southeastern Wyoming, in proximity to Sand Lake, Wyoming (41°27.280 N, 106°17.240 W), elevation ~3,110 m (Fig. 1). The dominant vegetation type surrounding Sand Lake is a mixture of spruce-fir (*Picea engelmannii* and *Abies lasiocarpa*) forests and large meadows with woodland encroachments, consisting of small clusters of spruce and/or fir trees. Spruce beetle attack has resulted in clusters of dying and dead trees distributed around the lake, representing the progression from healthy to dead (Fig. 1). This resulted in three different infestation stages being selected for sampling: healthy, infested, and dead, which were defined by the following criteria: healthy clusters were characterized by no visible signs of beetle infestation, infested clusters by visible bore holes and needles changing from green to red, and dead clusters by trees with no needles remaining. In an attempt to constrain time since attack, trees in dead clusters still retained bark and some fine branches and were standing upright.

Tree clusters ranging in size from two to eight trees were selected based upon several characteristics, including infestation stage, understory composition and cover, aspect, tree size, and proximity of clusters to trees representing a different infestation stage. In an attempt to isolate the effects of bark beetle-induced tree mortality on soil microbiota, tree clusters were selected with little to no understory and slope. In addition, clusters were chosen from the toe slope on the north and south sides of Sand Lake. All tree clusters were located in the woodland encroachment, as opposed to within densely forested stands. The use of small clusters of trees allowed for best possible isolation of a single infestation stage, with limited interference from nearby clusters of a different infestation stage. Trees had a minimum DBH (diameter at breast height; ~1.37 m) of 25 cm. A total of five to six clusters for each of the three infestation stages were selected in July 2016. The experimental design used was not completely spatially balanced and as such may not adequately account for space as a driver of difference among sites. With this, the distance between clusters, while often greater than 30 m, is as low as 11 m between two clusters of differing infestation stages, potentially contributing to similarity among sites (Fig. 1).

Soil collection and processing. Each cluster was sampled at two time points, once in the summer and once in early fall of 2016. At each time point, two separate soil samples were collected per cluster. A total of five healthy, six infested, and six dead clusters were sampled. The unequal number of clusters was caused by the inability to recover full soil cores at one dead and one infested cluster during the second time point. Therefore, one additional infested and dead cluster were selected based on the required characteristics, and two soil cores were taken from these clusters instead, resulting in the same number of samples per infestation stage ($n = 20$, for a total of 60 soil cores), but different numbers of clusters.

Prior to soil sampling, the litter layer (Oi horizon) was scraped away, and a 15-by-15-cm sample was collected to a depth of 10 cm using a square-point ethanol-sterilized shovel. Soil samples were collected from the middle of the tree cluster and included the organic horizon, comprised of the Oe and Oa horizons, with minimal contribution of the mineral horizon. Samples were placed into Ziploc bags, kept on ice for transportation back to the University of Wyoming, and stored at ~4°C until further processing. All samples were processed within 48 h of collection in order to limit changes in microbial community structure or nutrient status.

Soil samples were split into bulk and rhizosphere soil by first removing roots which could be directly traced to grasses, forbs, or shrubs in an attempt to limit nonspruce roots. Remaining fine roots were collected using sterilized forceps, lightly shaken to remove nonrhizosphere soil, and placed in a clean 50-ml Falcon tube. The tightly adhering rhizosphere soil was removed by dry vortexing the tube for approximately 90 s based on a previously published method (40). Though we acknowledge that this

method may have provided a less-complete extraction compared to a buffer extraction, we decided on the vortex method based on available resources, and it was deemed an acceptable method in the *Handbook of Methods Used in Rhizosphere Research* (40). In addition, it is possible that collected roots were not solely from the target spruce species and as such the rhizosphere samples could be conservatively thought of as representing the rhizosphere of the entire plant community of the cluster, and not specifically the spruce rhizosphere. A final cleaning step of the rhizosphere soil in the tube was completed by removing all remaining root fragments using sterilized forceps, and the soil remaining in the tube was defined as the spruce rhizosphere soil. We defined the rhizosphere as soil closely adhering to the roots regardless of whether or not the roots were alive or dead. Even though roots cease to deposit carbon into the soil via exudation, the roots now provide a different carbon source in the form of necromass and, as such, continue to influence this soil compartment. To collect the bulk soil, the remainder of the original soil sample was sieved through an ethanol-sterilized sieve (2-mm mesh), with the soil passing through the 2-mm mesh considered bulk soil. The two soils discussed above, rhizosphere and bulk, are referred to as soil origins from here on.

Soil analyses. Subsamples (~250 mg) of the bulk and rhizosphere soils were added to MoBio PowerSoil bead tubes (Mo Bio, Carlsbad, CA) for DNA extraction and frozen at −20°C until all samples were processed. A subsample of the bulk soil was frozen at −20°C to be used for enzyme analysis. The remaining bulk soil was bagged and kept at 4°C for further analysis, while the remainder of the rhizosphere soil was frozen at −20°C. A subsample of fresh bulk soil was dried at ~65°C for 48 h to estimate the gravimetric water content. Soil pH and electrical conductivity (EC) were measured using an Oakton PC700 benchtop meter (Oakton Instruments, Vernon Hills, IL) with a soil/deionized water ratio of 1:2 (wt/vol). The soil C:N ratio was determined on subsamples of freeze-dried and ground bulk soil on a Costech 4010 elemental analyzer (Costech Analytical Technologies, Valencia, CA) at the Stable Isotope Facility (University of Wyoming, Laramie, WY).

Extracellular enzyme activities (EEA) were measured for nine enzymes involved in the cycling of carbon (C), nitrogen (N), and phosphorus (P), as outlined previously (41–44). Measured enzymes included: β-glucosidase (BG), β-xylosidase (BX), α-glucosidase (AG), cellobiohydrolase (CBH), *N*-acetyl-β-glucosaminidase (NAG), acid phosphatase (PHOS), leucine aminopeptidase (LAP), peroxidases (PEROX), and phenol oxidase (PHENOX). To ensure nonlimiting substrate availability and maximum potential enzyme activity (V_{max}) (45), a preliminary assay was performed using four different substrate concentrations (ranging from 200 to 4,000 μM) at five different measurement times (1, 2, 4, 6, 8, and 10 h). These preliminary assays were performed on three soil samples that are representative of the expected variability in enzymatic activity. Briefly, a soil slurry was created by homogenizing 1 g of soil with 100 ml of sodium acetate buffer (50 mM [pH 5.2]) for 30 s using a Magic Bullet blender (Homeland Housewares LLC). Buffer pH was chosen to minimize difference between buffer and soil pH and represented the mean pH of all soil samples ($\pm$0.41 [standard deviation]). In a 96-well microplate, 200 μl of soil slurry homogenate was combined with 50 μl of substrate and incubated at 20°C for 10 h. Four technical replicates per soil sample were used to measure fluorescence or absorbance after addition of the substrates. Fluorescence was measured on a Synergy HTX multimode reader (BioTek Instruments, Inc., Winooski, VT) at an excitation wavelength of 360 nm and an emission wavelength of 450 nm for hydrolytic enzymes and at an absorbance of 450 nm for oxidative enzymes. Samples were corrected for background fluorescence or absorbance using a negative control (sample homogenate with buffer), as well as a quench control (sample homogenate with standards) to correct for interference of soil particles with fluorescence intensity. The oxidative enzyme activities of PEROX and PHENOX were measured using 25 mM L-3,4 dihydroxyphenylalanine (L-DOPA), with or without addition of 10 μl of 0.3% hydrogen peroxide, respectively. For hydrolytic enzymes, fluorescence conversions were based on measurements of standards (10 μM): 4-methylumbelliferone for BG, BX, AG, CBH, NAG, PHOS, and 7-amido-4-methylcoumarin hydrochloride for LAP. Oxidative enzyme activities were converted using an empirically determined extinction coefficient of 7.9 μmol^{-1}, as used in other studies (42, 44). Final enzyme activities were calculated using formulas outlined by DeForest (44) and are reported as nmol or μmol of substrate converted per hour per g soil dry mass (nmol/μmol h^{-1} g^{-1}). From the preliminary assay, the incubation time and substrate concentration producing the highest average enzyme activity were selected for each enzyme. This resulted in a single substrate concentration and incubation time to be used for each enzyme across all samples for final enzyme assays. Final enzyme assays for all samples were done in a similar manner as the preliminary assays, but using the substrate concentration and incubation time that resulted in the maximum potential enzyme activity (V_{max}).

Statistical analyses of edaphic and enzymatic data. In order to determine whether significant differences ($P < 0.05$) existed between infestation stages in soil pH, EC, carbon (C), nitrogen (N), C:N ratio, and gravimetric water content, we used generalized linear models with an inverse-Gaussian distribution and a link function defined as "1/mu^2" with the infestation stage as a fixed effect (46). For individual EEA, we used zero-inflated negative binomial generalized linear models and a log-link function with infestation stage as a fixed effect (46). Pairwise differences were determined using Tukey's honestly significant difference (HSD) test. A potential shortcoming in our statistical analysis stems from samples collected from a small space having some degree of nonindependence. However, instead of condensing samples, we treated our samples as independent due to the fact that the edaphic conditions were different for each soil sample. This independence was supported by the fact that the variances within a cluster were larger than the expected measurement error; thus, we decided that condensing samples would mask the influence of soil conditions. Due to the limited number of samples at each time point for bulk soil edaphic measurements, the effect size of sampling time was not estimated in our linear models.

Differences among enzyme activity profiles as a function of infestation stage and sampling time were determined using permutational multivariate analysis of variance (PERMANOVA), pairwise adonis testing with the Bonferroni correction of Bray-Curtis dissimilarities in the vegan package in R 3.3.2 (47). Enzymatic profiles were then visualized using nonmetric multidimensional scaling (NMDS) via ggplot2 (48).

Soil DNA extraction and amplicon library preparation. After all soil samples were processed, frozen bead tubes were thawed, and DNA was extracted according to the manufacturer's instructions (Mo Bio). DNA extracts were stored at −20°C until further processing. Both bacterial (16S) and fungal (internal transcribed spacer [ITS]) amplicon libraries were prepared using primers modified with 8-bp molecular identification indices. In order to amplify the V4 region of the bacterial 16S rRNA gene, the modified 515F (5′-GTGYCAGCMGCCGCGGTAA-3′) (49) and 806R (5′-GGACTACNVGGGTWTCTAAT-3′) (50) primers were used as tested by Walters et al. (51) to improve amplification of some archaeal and bacterial groups. For the ITS2 region of the fungal genome, the primers fITS7 (5′-GTGARTCATCGAATCTTTG-3′) (52) and ITS4 (5′-TCCTCCGCTTATTGATATGC-3′) (53) were used. The PCR conditions were as follows: 98 °C for 30 s, 30 cycles of 98°C for 10 s, 65°C (bacteria) or 60°C (fungi) for 10 s, 72°C for 8 s, and 72°C for 5 min. The 20-μl PCRs contained 0.2 μl of Phusion high-fidelity DNA polymerase, 4 μl of 5$\times$ Phusion Green HF buffer, 0.4 μl of deoxynucleoside triphosphates (10 mM), 12.4 μl of diethyl pyrocarbonate-water, 1 μl each of forward and reverse primer (10 μM), and 1 μl of template DNA. PCRs were performed in triplicate, and each amplification was verified on a 1.5% agarose gel. Positive and negative controls were included in each PCR. PCR products were combined and cleaned using Axygen's AxyPrep Mag PCR clean-up kit according to the manufacturer's instructions (Axygen Biosciences, Union City, CA). Concentrations of cleaned PCR products were measured using a dsDNA HS assay kit on a Qubit 3.0 fluorometer (Invitrogen/Life Technologies, Carlsbad, CA). An equimolar mix was prepared of the cleaned bacterial and fungal products separately for submission to the University of Minnesota Genomics Center and sequenced on the Illumina MiSeq platform using V2 chemistry (2 $\times$ 250 PE). Fungal and bacterial libraries were sequenced separately. No positive or negative controls were included in sequencing.

Sequence data analysis. Raw sequence data were analyzed in R v3.4.2 (54) using the DADA2 pipeline (55). Filtering and error learning steps were performed slightly differently for ITS and 16S data due to the inherent variable lengths of ITS reads. Reads were checked for remaining primers and removed using cutadapt v1.9 (56). ITS filtering and error learning used the following parameters: filterAndTrim(maxEE=1,1, truncQ=11, maxN=0, minLen=50, rm.phix=TRUE), while 16S filtering used filterAndTrim(truncLen=c(240,180), maxEE=2, truncQ=11, maxN=0, rm.phix=TRUE). One million reads were used to learn errors for both the ITS and 16S data and reads were clustered into amplicon sequence variants (ASVs). Chimeras were removed using DADA2's function removeBimeraDenovo, and taxonomy was assigned to each ASV (with a minimum bootstrap confidence of 80%) using the reference databases Silvia V128 (57) for bacteria and UNITE (58) for fungi. Downstream alpha- and beta-diversity analyses were performed using Phyloseq (59). Reads which did not assign to fungi or bacteria were removed, and the remaining data set was normalized to within-site proportional abundances to avoid rarefaction when possible. The within-sample proportional abundances were calculated by dividing the reads assigned to an ASV in a sample by the total number of reads for that sample. However, alpha-diversity and differential abundance analyses required rarefaction. Several samples were removed from the sequencing lane due to failed DNA extractions, PCR, or sequencing. The final fungal data set consisted of 20 healthy, 20 infested, and 19 dead samples for each of the soil origins (bulk and rhizosphere). For bacteria, the final data set consisted of 19 healthy, 18 infested, and 19 dead sites for bulk soil and 19 healthy, 15 infested, and 19 dead samples for the rhizosphere.

Statistical analysis of microbial community data. Shannon diversity and species richness were determined using rarefied data and the Phyloseq V 1.23.1 function estimate_richness. Statistical differences between infestation stages were determined using generalized linear models with an inverse-Gaussian distribution and a link function defined as "1/mu^2" with infestation stage as a fixed effect (46). Pairwise differences determined *post hoc* using Tukey's HSD test. Bray-Curtis pairwise dissimilarities of community data were visualized using NMDS, and significant differences between infestation stages, soil origins, and sampling times were determined using normalized data and PERMANOVA (pairwise adonis testing with Bonferroni correction). Sampling time and soil origin were included in the PERMANOVA testing but not in the linear modeling efforts due to the number of samples available for the estimation of variance. Approximately 15 samples per infestation state, soil origin, and time were available for the PERMANOVA testing, while for the linear modeling only ~2 samples for each time and soil origin were available within a cluster. Mantel testing was used to determine significant correlations between Bray-Curtis community dissimilarities, edaphic parameters, and geographic distances. Significant correlations between enzymatic activities, alpha-diversity, and total C, total N, and C:N were tested for using Spearman's correlation tests.

The DESeq2 package (60) was used to test for differential abundances of rarefied counts to define indicator species of 16S and ITS ASVs between the healthy and dead infestation stages at the genus level. The two stages were selected due to the fact that that they represented either end of the infestation spectrum and encompass the starting and end points of this study. Functional guilds and trophic modes were assigned to fungal taxa using FUNGuild (61). Only assignments with a confidence level of "possible," "probable," or "highly probable" were utilized for this analysis. Confidence levels falling below "possible" were converted to an unknown trophic or guild assignment. Taxa assigned as ectomycorrhizal were considered a subset, and alpha-diversity metrics were examined in similar fashion to the entire data set. We used zero-inflated negative binomial generalized linear models and a log-link function with infestation stage as a fixed effect (46) to determine significant differences ($\alpha = 0.05$) in abundance of trophic

modes among infestation stages for rarefied relative abundances. Pairwise differences were determined *post hoc* using Tukey's HSD test.

Data availability. Raw sequence reads and metadata are available under the SRA BioProject number PRJNA552356. Phyloseq objects containing ESV tables, metadata, and taxonomic assignments are available at https://doi.org/10.5281/zenodo.3369974.

ACKNOWLEDGMENTS

We thank Shannon Albeke for producing our maps, and we thank three anonymous reviewers for their thoughtful comments and suggestions.

Support for this research was provided through the University of Wyoming's Plant Sciences departmental graduate assistantships and the Microbial Ecology Collaborative with funding from National Science Foundation (NSF) award no. EPS-1655726.

REFERENCES

1. Fettig CJ, Klepzig KD, Billings RF, Munson AS, Nebeker TE, Negrón JF, Nowak JT. 2007. The effectiveness of vegetation management practices for prevention and control of bark beetle infestations in coniferous forests of the western and southern United States. For Ecol Manage 238:24–53. https://doi.org/10.1016/j.foreco.2006.10.011.
2. Hebertson EG, Jenkins MJ. 2008. Climate factors associated with historic spruce beetle (Coleoptera: Curculionidae) outbreaks in Utah and Colorado. Environ Entomol 37:281–292. https://doi.org/10.1093/ee/37.2.281.
3. Bentz BJ, Régnière J, Fettig CJ, Hansen EM, Hayes JL, Hicke JA, Kelsey RG, Negrón JF, Seybold SJ. 2010. Climate change and bark beetles of the western United States and Canada: direct and indirect effects. Bioscience 60:602–613. https://doi.org/10.1525/bio.2010.60.8.6.
4. Jenkins M, Hebertson E, Munson A. 2014. Spruce beetle biology, ecology, and management in the Rocky Mountains: an addendum to spruce beetle in the Rockies. Forests 5:21–71. https://doi.org/10.3390/f5010021.
5. Morehouse K, Johns T, Kaye J, Kaye M. 2008. Carbon and nitrogen cycling immediately following bark beetle outbreaks in southwestern ponderosa pine forests. For Ecol Manage 255:2698–2708. https://doi.org/10.1016/j.foreco.2008.01.050.
6. Edburg SL, Hicke JA, Lawrence DM, Thomton PE. 2011. Simulating coupled carbon and nitrogen dynamics following mountain pine beetle outbreaks in the western United States. J Geophys Res 116:1–15.
7. Mikkelson KM, Bearup LA, Maxwell RM, Stednick JD, McCray JE, Sharp JO. 2013. Bark beetle infestation impacts on nutrient cycling, water quality, and interdependent hydrological effects. Biogeochemistry 115:1–21. https://doi.org/10.1007/s10533-013-9875-8.
8. Cigan PW, Karst J, Cahill JF, Sywenky AN, Pec GJ, Erbilgin N. 2015. Influence of bark beetle outbreaks on nutrient cycling in native pine stands in western Canada. Plant Soil 390:29–47. https://doi.org/10.1007/s11104-014-2378-0.
9. Norton U, Ewers BE, Borkhuu B, Brown NR, Pendall E. 2015. Soil nitrogen five years after bark beetle infestation in lodgepole pine forests. Soil Sci Soc Am J 79:282–293. https://doi.org/10.2136/sssaj2014.05.0223.
10. Štursová M, Šnajdr J, Cajthaml T, Bárta J, Šantrůčková H, Baldrian P. 2014. When the forest dies: the response of forest soil fungi to a bark beetle-induced tree dieback. ISME J 8:1920–1931. https://doi.org/10.1038/ismej.2014.37.
11. Hañáčkova Z, Koukol O, Štursová M, Kolařík M, Baldrian P. 2015. Fungal succession in the needle litter of a montane Picea abies forest investigated through strain isolation and molecular fingerprinting. Fungal Ecol 13:157–166. https://doi.org/10.1016/j.funeco.2014.09.007.
12. Pec GJ, Karst J, Taylor DL, Cigan PW, Erbilgin N, Cooke JEK, Simard SW, Cahill JF. 2017. Change in soil fungal community structure driven by a decline in ectomycorrhizal fungi following a mountain pine beetle (*Dendroctonus ponderosae*) outbreak. New Phytol 213:864–873. https://doi.org/10.1111/nph.14195.
13. Mikkelson KM, Bokman CM, Sharp JO. 2016. Rare taxa maintain microbial diversity and contribute to terrestrial community dynamics throughout bark beetle infestation. Appl Environ Microbiol 82:6912–6919. https://doi.org/10.1128/AEM.02245-16.
14. Mikkelson KM, Lozupone CA, Sharp JO. 2016. Altered edaphic parameters couple to shifts in terrestrial bacterial community structure associated with insect-induced tree mortality. Soil Biol Biochem 95:19–29. https://doi.org/10.1016/j.soilbio.2015.12.001.
15. Ferrenberg S, Knelman JE, Jones JM, Beals SC, Bowman WD, Nemergut DR. 2014. Soil bacterial community structure remains stable over a 5-year chronosequence of insect-induced tree mortality. Front Microbiol 5:1–11.
16. Crowther TW, Thomas SM, Maynard DS, Baldrian P, Covey K, Frey SD, van Diepen LTA, Bradford MA. 2015. Biotic interactions mediate soil microbial feedbacks to climate change. Proc Natl Acad Sci U S A 112:7033–7038. https://doi.org/10.1073/pnas.1502956112.
17. Bulgarelli D, Schlaeppi K, Spaepen S, Ver Loren van Themaat E, Schulze-Lefert P. 2013. Structure and functions of the bacterial microbiota of plants. Annu Rev Plant Biol 64:807–838. https://doi.org/10.1146/annurev-arplant-050312-120106.
18. Baldrian P. 2017. Forest microbiome: diversity, complexity and dynamics. FEMS Microbiol Rev 41:109–130. https://doi.org/10.1093/femsre/fuw040.
19. Hopkins AJM, Ruthrof KX, Fontaine JB, Matusick G, Dundas SJ, Hardy GEs. 2018. Forest die-off following global-change-type drought alters rhizosphere fungal communities. Environ Res Lett 13:095006. https://doi.org/10.1088/1748-9326/aadc19.
20. Bahram M, Hildebrand F, Forslund SK, Anderson JL, Soudzilovskaia NA, Bodegom PM, Bengtsson-Palme J, Anslan S, Coelho LP, Harend H, Huerta-Cepas J, Medema MH, Maltz MR, Mundra S, Olsson PA, Pent M, Põlme S, Sunagawa S, Ryberg M, Tedersoo L, Bork P. 2018. Structure and function of the global topsoil microbiome. Nature 560:233–237. https://doi.org/10.1038/s41586-018-0386-6.
21. Peay KG, von Sperber C, Cardarelli E, Toju H, Francis CA, Chadwick OA, Vitousek PM. 2017. Convergence and contrast in the community structure of Bacteria, Fungi and Archaea along a tropical elevation-climate gradient. FEMS Microbiol Ecol 93:1–12.
22. Keville MP, Reed SC, Cleveland CC. 2013. Nitrogen cycling responses to mountain pine beetle disturbance in a high elevation whitebark pine ecosystem. PLoS One 8:e65004-8. https://doi.org/10.1371/journal.pone.0065004.
23. Brand DG, Kehoe P, Connors M. 1986. Coniferous afforestation leads to soil acidification in central Ontario. Can J for Res 16:1389–1391. https://doi.org/10.1139/x86-248.
24. Brouillard BM, Mikkelson KM, Bokman CM, Berryman EM, Sharp JO. 2017. Extent of localized tree mortality influences soil biogeochemical response in a beetle-infested coniferous forest. Soil Biol Biochem 114:309–318. https://doi.org/10.1016/j.soilbio.2017.06.016.
25. Lindahl BD, Ihrmark K, Boberg J, Trumbore SE, Högberg P, Stenlid J, Finlay RD. 2007. Spatial separation of litter decomposition and mycorrhizal nitrogen uptake in a boreal forest. New Phytol 173:611–620. https://doi.org/10.1111/j.1469-8137.2006.01936.x.
26. Bödeker ITM, Clemmensen KE, de Boer W, Martin F, Olson Å, Lindahl BD. 2014. Ectomycorrhizal *Cortinarius* species participate in enzymatic oxidation of humus in northern forest ecosystems. New Phytol 203:245–256. https://doi.org/10.1111/nph.12791.
27. Talbot JM, Bruns TD, Taylor JW, Smith DP, Branco S, Glassman SI, Erlandson S, Vilgalys R, Liao H-L, Smith ME, Peay KG. 2014. Endemism and functional convergence across the North American soil mycobiome. Proc Natl Acad Sci U S A 111:6341–6346. https://doi.org/10.1073/pnas.1402584111.
28. Hanson CA, Allison SD, Bradford MA, Wallenstein MD, Treseder KK. 2008. Fungal taxa target different carbon sources in forest soil. Ecosystems 11:1157–1167. https://doi.org/10.1007/s10021-008-9186-4.
29. Lindahl BD, Tunlid A. 2015. Ectomycorrhizal fungi: potential organic matter decomposers, yet not saprotrophs. New Phytol 205:1443–1447. https://doi.org/10.1111/nph.13201.

30. Talbot JM, Allison SD, Treseder KK. 2008. Decomposers in disguise: mycorrhizal fungi as regulators of soil C dynamics in ecosystems under global change. Funct Ecol 22:955–963. https://doi.org/10.1111/j.1365-2435.2008.01402.x.
31. Shah F, Nicolás C, Bentzer J, Ellström M, Smits M, Rineau F, Canbäck B, Floudas D, Carleer R, Lackner G, Braesel J, Hoffmeister D, Henrissat B, Ahrén D, Johansson T, Hibbett DS, Martin F, Persson P, Tunlid A. 2016. Ectomycorrhizal fungi decompose soil organic matter using oxidative mechanisms adapted from saprotrophic ancestors. New Phytol 209:1705–1719. https://doi.org/10.1111/nph.13722.
32. Vaario L-M, Heinonsalo J, Spetz P, Pennanen T, Heinonen J, Tervahauta A, Fritze H. 2012. The ectomycorrhizal fungus *Tricholoma matsutake* is a facultative saprotroph *in vitro*. Mycorrhiza 22:409–418. https://doi.org/10.1007/s00572-011-0416-9.
33. Kuyper TW. 2017. Carbon and energy sources of mycorrhizal fungi, p 357–374. *In* Mycorrhizal mediation of soil. Elsevier, New York, NY.
34. Walker JKM, Ward V, Paterson C, Jones MD. 2012. Coarse woody debris retention in subalpine clearcuts affects ectomycorrhizal root tip community structure within fifteen years of harvest. Appl Soil Ecol 60:5–15. https://doi.org/10.1016/j.apsoil.2012.02.017.
35. Lladó S, López-Mondéjar R, Baldrian P. 2017. Forest soil bacteria: diversity, involvement in ecosystem processes, and response to global change. Microbiol Mol Biol Rev 81:1–27.
36. Dennis PG, Miller AJ, Hirsch PR. 2010. Are root exudates more important than other sources of rhizodeposits in structuring rhizosphere bacterial communities? FEMS Microbiol Ecol 72:313–327. https://doi.org/10.1111/j.1574-6941.2010.00860.x.
37. Lauber CL, Hamady M, Knight R, Fierer N. 2009. Pyrosequencing-based assessment of soil pH as a predictor of soil bacterial community structure at the continental scale. Appl Environ Microbiol 75:5111–5120. https://doi.org/10.1128/AEM.00335-09.
38. Štursová M, Baldrian P. 2011. Effects of soil properties and management on the activity of soil organic matter transforming enzymes and the quantification of soil-bound and free activity. Plant Soil 338:99–110. https://doi.org/10.1007/s11104-010-0296-3.
39. Cenini VL, Fornara DA, McMullan G, Ternan N, Carolan R, Crawley MJ, Clément J-C, Lavorel S. 2016. Linkages between extracellular enzyme activities and the carbon and nitrogen content of grassland soils. Soil Biol Biochem 96:198–206. https://doi.org/10.1016/j.soilbio.2016.02.015.
40. Luster J, Finlay R. 2006. Handbook of methods used in rhizosphere research. Swiss Federal Research Institute WSL, Birmensdorf, Switzerland.
41. Bell CW, Fricks BE, Rocca JD, Steinweg JM, McMahon SK, Wallenstein MD. 2013. High-throughput fluorometric measurement of potential soil extracellular enzyme activities. J Vis Exp 2013:1–16.
42. Saiya-Cork K, Sinsabaugh R, Zak D. 2002. The effects of long-term nitrogen deposition on extracellular enzyme activity in an *Acer saccharum* forest soil. Soil Biol Biochem 34:1309–1315. https://doi.org/10.1016/S0038-0717(02)00074-3.
43. Van Diepen LTA, Frey SD, Sthultz CM, Morrison EW, Minocha R, Pringle A. 2015. Changes in litter quality caused by simulated nitrogen deposition reinforce the N-induced suppression of litter decay. Ecosphere 6:art205-16. https://doi.org/10.1890/ES15-00262.1.
44. DeForest JL. 2009. The influence of time, storage temperature, and substrate age on potential soil enzyme activity in acidic forest soils using MUB-linked substrates and l-DOPA. Soil Biol Biochem 41:1180–1186. https://doi.org/10.1016/j.soilbio.2009.02.029.
45. German DP, Weintraub MN, Grandy AS, Lauber CL, Rinkes ZL, Allison SD. 2011. Optimization of hydrolytic and oxidative enzyme methods for ecosystem studies. Soil Biol Biochem 43:1387–1397. https://doi.org/10.1016/j.soilbio.2011.03.017.
46. Venables WN, Ripley BD. 2002. Package 'MASS': modern applied statistics with S. https://cran.r-project.org/web/packages/MASS/MASS.pdf.
47. Oksanen J, Blanchet FG, Friendly M, Kindt R, Legendre P, McGlinn D, Minchin PR, O'Hara R, Gavin L, Simpson P, Solymos M, Stevens HH, Szoecs E, Wagner H. 2017. vegan: community ecology package. R package version 2.4-3. https://cran.r-project.org/web/packages/vegan/vegan.pdf.
48. Wickham H. 2009. ggplot2: elegant graphics for data analysis. Springer-Verlag, New York, NY.
49. Parada AE, Needham DM, Fuhrman JA. 2016. Every base matters: assessing small subunit rRNA primers for marine microbiomes with mock communities, time series, and global field samples. Environ Microbiol 18:1403–1414. https://doi.org/10.1111/1462-2920.13023.
50. Apprill A, Mcnally S, Parsons R, Weber L. 2015. Minor revision to V4 region SSU rRNA 806R gene primer greatly increases detection of SAR11 bacterioplankton. Aquat Microb Ecol 75:129–137. https://doi.org/10.3354/ame01753.
51. Walters W, Hyde ER, Berg-Lyons D, Ackermann G, Humphrey G, Parada A, Gilbert JA, Jansson JK, Caporaso JG, Fuhrman JA, Apprill A, Knight R. 2016. Improved bacterial 16S rRNA gene (V4 and V4-5) and fungal internal transcribed spacer marker gene primers for microbial community surveys. mSystems 1:e00009-15.
52. Ihrmark K, Bödeker ITM, Cruz-Martinez K, Friberg H, Kubartova A, Schenck J, Strid Y, Stenlid J, Brandström-Durling M, Clemmensen KE, Lindahl BD. 2012. New primers to amplify the fungal ITS2 region: evaluation by 454-sequencing of artificial and natural communities. FEMS Microbiol Ecol 82:666–677. https://doi.org/10.1111/j.1574-6941.2012.01437.x.
53. White TJ, Bruns T, Lee S, Taylor J. 1990. Amplification and direct sequencing of fungal ribosomal RNA genes for phylogenetics, p 315–322. *In* PCR protocols. Elsevier, New York, NY.
54. R Core Team. 2018. R: a language and environment for statistical computing. R Core Team, Vienna, Austria.
55. Callahan BJ, McMurdie PJ, Rosen MJ, Han AW, Johnson AJA, Holmes SP. 2016. DADA2: high-resolution sample inference from Illumina amplicon data. Nat Methods 13:581–583. https://doi.org/10.1038/nmeth.3869.
56. Martin M. 2011. Cutadapt removes adapter sequences from high-throughput sequencing reads. EMBNET J 17:10. https://doi.org/10.14806/ej.17.1.200.
57. Quast C, Pruesse E, Yilmaz P, Gerken J, Schweer T, Yarza P, Peplies J, Glöckner FO. 2013. The SILVA ribosomal RNA gene database project: improved data processing and web-based tools. Nucleic Acids Res 41:D590–D596. https://doi.org/10.1093/nar/gks1219.
58. Abarenkov K, Nilsson RH, Larsson KH, Alexander IJ, Eberhardt U, Erland S, Høiland K, Kjøller R, Larsson E, Pennanen T, Sen R, Taylor AFS, Tedersoo L, Ursing BM, Vrålstad T, Liimatainen K, Peintner U, Kõljalg U. 2010. The UNITE database for molecular identification of fungi - recent updates and future perspectives. New Phytol 186:281–285. https://doi.org/10.1111/j.1469-8137.2009.03160.x.
59. McMurdie PJ, Holmes S. 2013. phyloseq: an R package for reproducible interactive analysis and graphics of microbiome census data. PLoS One 8:e61217. https://doi.org/10.1371/journal.pone.0061217.
60. Love MI, Huber W, Anders S. 2014. Moderated estimation of fold change and dispersion for RNA-seq data with DESeq2. Genome Biol 15:550. https://doi.org/10.1186/s13059-014-0550-8.
61. Nguyen NH, Song Z, Bates ST, Branco S, Tedersoo L, Menke J, Schilling JS, Kennedy PG. 2016. FUNGuild: an open annotation tool for parsing fungal community datasets by ecological guild. Fungal Ecol 20:241–248. https://doi.org/10.1016/j.funeco.2015.06.006.